NMR Study of Ion-Conducting Organic−Inorganic Nanocomposites Poly(ethylene glycol)−Silica−$LiClO_4$

Nilson C. Mello,[†] Tito J. Bonagamba,*[,†] Horácio Panepucci,[†] Karim Dahmouche,[‡] Patrick Judeinstein,[§] and Michel A. Aegerter[||]

Instituto de Física de São Carlos, Universidade de São Paulo, Caixa Postal 369, CEP: 13560-970, São Carlos-SP, Brazil; Instituto de Química de Araraquara-UNESP, Av. Prof. Francisco Degni s/n, CEP: 14800−900, Araraquara-SP, Brazil; Laboratoire de Chimie Structurale Organique, UPRESA CNRS 8074, Université Paris-Sud, 91405 Orsay, France; Institut für Neue Materialien-Department of Coating Technology, Im Stadtwald, Gebäude 43, D-66123, Saarbrücken, Germany

Received September 24, 1999; Revised Manuscript Received December 30, 1999

ABSTRACT: Hybrid organic−inorganic ionic conductors, also called ormolytes, were obtained by dissolution of $LiClO_4$ into silica/poly(ethylene glycol) matrices. Solid-state nuclear magnetic resonance (NMR) was used to probe the inorganic phase structure (^{29}Si) and the effects of the temperature and composition on the dynamic behavior of the ionic species (^{7}Li) and the polymer chains (^{1}H and ^{13}C). The NMR results between −100 and +90 °C show a strong correlation with ionic conductivity and differential scanning calorimetry experiments. The results also demonstrate that the cation mobility is assisted by segmental motion of the polymer, which is in agreement with the results previously reported for pure poly(ethylene oxide), PEO, electrolytes.

Introduction

Over the past few years, many studies have been reported in the field of solid polymer electrolytes.[1] These promising materials are of potential interest for various applications such as batteries, data storage, sensors, and electrochromic and photoelectrochemical devices.[2] Systems showing ionic conductivity induced by the addition of lithium salts offer the most favorable properties.[3] It is well-established in pure polymer electrolytes that conductivity occurs in the amorphous phase, above the glass transition temperature (T_g), via a liquidlike motion of the cations associated with segmental reorientations of the neighboring chains.[1,4,5] Increasing the volume fraction of the amorphous domains and decreasing its T_g appear to be the main rules to obtain better ionic conductivity.

Recently organic−inorganic hybrids or nanocomposite systems (also called ormolytes—organically modified electrolytes) were demonstrated to be excellent polymer electrolytes. Such materials are constituted of organic (polymer) and inorganic (silica) phases mixed at the nanometric scale, leading to materials with new properties such as transparency and high mechanical strength.[6−11] The sol−gel route[12] is a unique way to design such structures because this room temperature process allows synthesis of an inorganic network under mild conditions. The ormolyte properties are strongly dependent on the connectivity of the two phases and the mobility of both the structural network and the active ionic species. This connectivity can be partially controlled by the chemistry, leading to two main families.[13] In type I nanocomposites, hydrogen bonds and van der Waals interactions associate the organic and inorganic components, while in type II materials, these two phases are linked together through covalent bonds. Inorganic salts can be dissolved in both types of materials, resulting in good ionic conductors.

The enhancement of the properties of these materials must be based on the knowledge of the microscopic molecular phenomenon, and nuclear magnetic resonance (NMR) yields notable contributions. This work reports a ^{1}H, ^{7}Li, ^{13}C, and ^{29}Si solid-state NMR study of new hybrid ionic conductors based on SiO_2−poly(ethylene glycol) networks of type I and type II doped with lithium perchlorate ($LiClO_4$). NMR is used to study the motion of both the mobile cation and the polymer backbone through the measurement of line widths, $\Delta\nu$, and spin−lattice relaxation times, T_1. Differential scanning calorimetry (DSC) was used to identify the glass transition temperatures,[14,15] and previous ionic conductivity results[16,17] are included for further discussion and to elucidate the influence of the material type and composition on their properties.

Materials and Methods

Sample Preparation. All chemical reagents are commercially available (Fluka, Aldrich), were used without further purification, and contain all nuclei at natural isotopic abundance. Materials of type I were prepared by an ultrasonic method:[16,17] 12.5 mL of tetraethoxysilane (TEOS) and 4 mL of water were stirred together under ultrasound to hydrolyze the TEOS. Then the desired quantities of poly(ethylene glycol), $HO(CH_2CH_2O)_nH$, PEG, with various molecular weights (PEG_n, n = number of ethylene oxide monomers) were added under neutral pH conditions. $LiClO_4$ was then introduced and dissolved using ultrasound in order to obtain a transparent monophasic liquid. Gelation occurred in a few minutes and the samples were slowly dried at 90 °C as a monolithic solid piece. This method is very similar to the sol−gel method used previously to prepare type I nanocomposite samples, with the exception of the ultrasonic activation. Only weak interactions are expected to link together the organic and inorganic components in these materials.[9,14,18]

* To whom correspondence should be addressed. Present address: Polymer Science and Engineering Department, University of Massachusetts, Amherst, Massachusetts, 01003. Telephone: (413) 577−1436. Fax: (413) 545−0082. E-mail: tito@polysci.umass.edu **or** tito@if.sc.usp.br.

[†] Universidade de São Paulo.

[‡] Instituto de Química de Araraquara-UNESP.

[§] Université Paris-Sud.

[||] Institut für Neue Materialien-Department of Coating Technology.

10.1021/ma991624w CCC: $19.00
Published on Web 01/31/2000

Table 1. Ormolytes of Types I and II, and Silica-Free Samples

series 1	series 2	series 3	series 4	series 5	series 6	series 7
$[41]_6$[4]-I	$[58]_6$[4]-I	$[58]_6$[4]-I	$[26]_2$[4]-II	$[76]_{17}$[4]-II	$[100]_6$[4]	$[100]_6$[30]
$[58]_6$[4]-I	$[58]_{12}$[4]-I	$[58]_6$[8]-I	$[76]_{17}$[4]-II	$[76]_{17}$[8]-II	$[100]_{12}$[4]	$[100]_{12}$[30]
$[73]_6$[4]-I	$[58]_{20}$[4]-I	$[58]_6$[10]-I	$[83]_{42}$[4]-II	$[76]_{17}$[10]-II	$[100]_{20}$[4]	$[100]_{20}$[30]
$[78]_6$[4]-I		$[58]_6$[15]-I	$[76]_{17}$[15]-II	$[76]_{17}$[15]-II		
$[83]_6$[4]-I		$[58]_6$[30]-I	$[83]_{42}$[15]-II	$[76]_{17}$[30]-II		
$[91]_6$[4]-I		$[58]_6$[80]-I				
$[95]_6$[4]-I						

The synthesis of PEG/silica type II was already described elsewhere.[10,14,16,17] Equimolar amounts of 3-isocyanatopropyltriethoxysilane (IsoTrEOS) and *O,O′*-bis(2-aminopropyl) poly(ethylene glycol) (abbreviation: $NH_2-PEG-NH_2$) were stirred together in tetrahydrofuran (THF) and refluxed for 6 h. THF was evaporated and a pure hybrid precursor $(OEt)_3Si-NH-PEG-NH-Si(OEt)_3$ was obtained. Afterward, 0.5 g of this precursor was mixed with 1 mL of ethanol containing NH_4F ($NH_4F/Si = 0.005$) to which was added the desired quantities of $LiClO_4$. Finally, 0.2 mL of water was added under vigorous stirring. A monolithic gel was obtained after 4 h. The ethanol was then slowly removed under vacuum at 90 °C to yield a piece of rubbery material. The existence of covalent chemical bonds between the silica network and the polymer chains has been reported for similar materials.[8,10,14] The thermal history is the same for all samples. After the preparation, the nanocomposites were immediately sealed in appropriate glass tubes for NMR and aluminum pans for DSC.

Other important alkali metal salts could have been used to prepare these ionic conducting systems, for example: $LiCF_3SO_3$ or $NaClO_4$. However, either the cation possesses a higher quadrupolar moment than ^{7}Li ($I = 3/2$), e.g., ^{23}Na ($I = 3/2$), or their anions contain high natural abundance and intense magnet moment nuclei, e.g., ^{19}F ($I = 1/2$). To avoid additional nuclear interactions and simplify the interpretation of the cation NMR measurements we decided to use $LiClO_4$. ^{7}Li possesses one of the smallest quadrupolar moments and the counterion ClO_4^- contains magnetic nuclei with relatively low abundances and small magnetic moments. However, it was not possible to study in this work the dynamics of the ClO_4^- anion and its correlation with the polymer chain motion due to the low NMR sensitivity and high electric quadrupole moments of the ^{35}Cl and ^{17}O nuclei.

The following nomenclature will be used to describe the composites: $[X]_n[Y]$-*Z*, where *X* represents the weight percent of polymer, *n* the average number of monomers in each polymer chain, and *Y* the ratio [O]/[Li] (where the oxygens considered are only those of the ether type), and *Z* equals I or II, for the corresponding type of ormolyte, nonbonded and chemically bonded, respectively.

Silica-free samples of $LiClO_4$-doped PEG_n were also prepared. They were obtained by direct dissolution, at 50 °C, of appropriate amounts of $LiClO_4$ in the polymer to obtain the desired value of *Y*. The nomenclature of these materials is the same as used above, however in this case $[X] = 100$.

Seven different series of samples were prepared as listed in Table 1. Series 1, 2, and 3 are composed of nonbonded samples (type I). In each of these different series only one of the parameters was varied, respectively *X*, *n*, and *Y*, while the others remained constant. Series 4 consists of bonded samples (type II) having different combinations of *X* and *n*. The values of *X* and *n* in type II nanocomposites are codependent. In series 5, the influence of the oxygen-to-lithium ratio, [*Y*], in type II samples is studied. Finally, series 6 and 7 consist of silica-free samples having different values of *n* for *Y* equaling 4 and 30, respectively.

Experimental Techniques

Solid-State NMR. Room-temperature solid-state ^{29}Si ($I = 1/2$) NMR measurements were performed in order to determine the structure of the inorganic component inside the different materials. ^{7}Li ($I = 3/2$), ^{13}C ($I = 1/2$), and ^{1}H ($I = 1/2$) NMR measurements were performed as a function of the temperature with the purpose of establishing relationships between the sample preparation conditions and the dynamic properties of both the Li^+ ion and the polymer chain. Solid-state NMR spectra were recorded between −100 and +90 °C at 2 T using a TECMAG LIBRA system and a variable temperature double resonance Doty probe. The Larmor frequencies, ν_L, for ^{29}Si, ^{13}C, ^{7}Li, and ^{1}H are, respectively, 16.9, 21.4, 33.1, and 85.1 MHz. In all cases the spectra were obtained from the Fourier transform of the free induction decays (FID) following a single 10 μs $\pi/2$ excitation and a dead time of 10 μs. Magic-angle spinning (MAS) of the samples at 3 kHz was employed for obtaining ^{1}H,^{13}C, and ^{29}Si spectra. For ^{13}C and ^{29}Si nuclei, proton decoupling was always used during acquisition, while ^{7}Li spectra were successively acquired with and without proton decoupling. Special care was taken to avoid the sample heating due to RF irradiation by using long repetition times (normally ≥3 s) and a small number of averages.

The full width at half-height (fwhh) of the ^{1}H, ^{7}Li, and ^{13}C lines will be defined as the line width in this article. The spin−lattice relaxation times T_1 were measured for ^{7}Li, ^{13}C, and ^{1}H by the inversion−recovery method.[19] ^{1}H decoupling was used only during the ^{7}Li FID acquisition to improve the signal-to-noise ratio, thus allowing T_1 measurements over extended temperature and lithium concentration ranges.

In the case of the quadrupolar nucleus ^{7}Li ($I = 3/2$), the spin−lattice relaxation should be described by a distribution of two or more exponentials functions.[20,21] However, deviations from a single-exponential function are often hard to detect,[22,23] as was also found in this study. For all samples and temperatures the ^{7}Li T_1 was calculated using only one exponential function.

Because of the high sensitivity for ^{7}Li and ^{1}H NMR measurements, the uncertainties in the obtained values for ^{7}Li and ^{1}H line widths and spin−lattice relaxation times are around 5%. For the ^{13}C NMR experiments these uncertainties increase to 15%.

Ionic Conductivity. The electrical properties of the samples were analyzed by complex impedance spectroscopy between 20 and 100 °C with a Solartron 1260 apparatus, in the frequency range of 1 Hz to 10 MHz, and an applied voltage of 5 mV. The samples were monolithic pieces of about 0.5 mm thick, with flat surfaces. The contacts were made with plasticized conductive probes (Altoflex) pressed on the sample. Reproducible values of the ionic conductivity, σ, were obtained after drying the samples under vacuum at 90 °C for 24 h. Values of σ up to 10^{-3} S/cm were found at room temperature. The uncertainties in the obtained values for ionic conductivities are approximately 10%.

Differential Scanning Calorimetry (DSC). DSC measurements were performed on several samples with a scan rate of 10 °C/min from −80 to +90 °C using a Texas Instruments model 2910 apparatus.

NMR Background. The line width and spin−lattice relaxation NMR measurements as a function of the temperature yield information on Li^+ and polymer dynamics due to the motion-dependent anisotropic nuclear spin interactions. Two important parameters are obtained directly from NMR measurements of the solid polymer electrolytes as a function of the temperature. The first parameter is the temperature at which the NMR line width undergoes a strong narrowing phenomenon. The line width indicates the occurrence of low-frequency motions (1−100 kHz) that modulate the longitudinal local fields leading to an average of the interactions. The line width transition is then commonly associated with the increase in chain motion that occurs near the polymer glass transition, T_g. However, the agreement of T_g values from various different

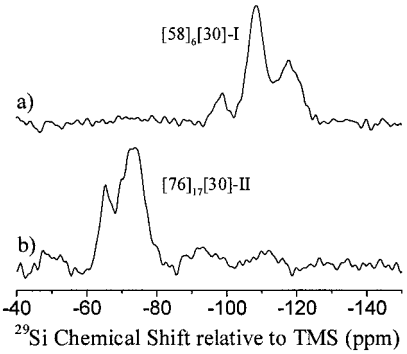

Figure 1. Typical ^{29}Si spectra for nonbonded and bonded ormolytes obtained at room temperature: (a) $[58]_6$[30]-I and (b) $[76]_{17}$[30]-II.

methods is poor, and the fact that they occur at about the same temperature may be coincidence. Part of this difficulty is due to the large difference in frequencies at which the information was obtained.[24−26] For this reason we shall use T_g^{NMR} to refer to the temperature at which the strongest change in NMR line width occurs. The second information is provided by the spin−lattice relaxation rate, T_1^{-1}, that reaches a maximum which is generally measured at a higher temperature ($> T_g^{NMR}$). This temperature, which we shall call T_{max}, corresponds to the condition where the transverse local field fluctuations achieve sufficient amplitude at the Larmor frequency to maximize the spin−lattice relaxation rate. The experimental uncertainty for T_{max} is ±2 °C. Both parameters T_g^{NMR} and T_{max} indicate the mobility of the polymer. The higher these two temperatures, the more rigid are the polymers.

Another important dynamic parameter can be indirectly obtained from the NMR data: the activation energy E_a. This parameter can be estimated using the Bloembergen, Purcell, and Pound (BPP) model[27−30] and the Arrhenius law. Using the well-known procedures for the determination of the activation energies,[22,31−33] this parameter can be evaluated for both relaxation processes.

Results and Discussion

^{29}Si NMR. The ^{29}Si NMR solid-state MAS spectra were used to characterize the silicon condensation and to indicate the silica network architecture inside these materials. Previously reported architectures include polymeric chains or compact clusters.[34,35] Nonbonded samples, type I, are obtained through the hydrolysis of tetraalkoxysilane ($Si(OEt_4)$), and then, in the silica phase, each silicate group is bonded to 1, 2, 3, or 4 other silicates through oxygen bridges. The notation Q^n (n = 1, 2, 3, or 4) is used to represent the number of connections that each silicate makes to its neighbors, i.e., $Si^*(OSi)_n(OX)_{4-n}$ (X = H or C) structural units. The ^{29}Si isotropic chemical shifts of the Q^n units are approximately −80, −87, −98, and −108 ppm (relative to tetramethylsilane = TMS), respectively for n = 1, 2, 3, or 4. When the degree of condensation is not high, inorganic polymer structures are predominant, with mainly Q^1 and Q^2 structures, while for three-dimensional agglomerates Q^3 and Q^4 structures prevail. The typical ^{29}Si spectrum obtained for the nonbonded ormolytes (type I) is illustrated by Figure 1a. The spectrum shows lines situated in the range between −100 and −120 ppm, associated with the Q^3 and Q^4 environments, indicating the dominant presence of silica agglomerates. This spectrum is similar to those of type I materials obtained under acidic conditions without $LiClO_4$.[18]

Figure 1b presents the typical ^{29}Si spectrum of type II nanocomposites with lines centered around −65 and

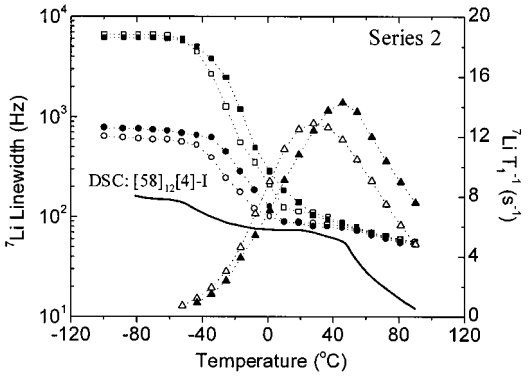

Figure 2. Temperature dependence of the ^{7}Li spin−lattice relaxation rate and line width, with and without ^{1}H decoupling, for the nanocomposites belonging to series 2 in Table 1 with n = 6 and 20. For comparison, the continuous line represents the DSC curve for the sample $[58]_{12}$[4]-I with arbitrary units along the y axis. Key: (□) $[58]_6$[4]-I-$\Delta\nu$; (○) $[58]_6$[4]-I-$\Delta\nu_{dec}$; (■) $[58]_{20}$[4]-I-$\Delta\nu$; (●) $[58]_{20}$[4]-I-$\Delta\nu_{dec}$; (△) $[58]_6$[4]-I-T_1^{-1}; (▲) $[58]_{20}$[4]-I-T_1^{-1}. The uncertainties in the ^{7}Li spin−lattice relaxation rates and line widths are approximately 5%.

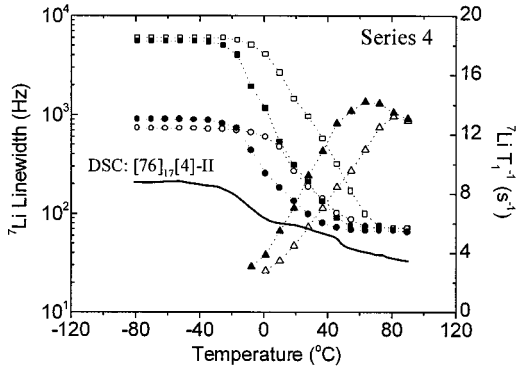

Figure 3. Temperature dependence of the ^{7}Li spin−lattice relaxation rate and line width, with and without ^{1}H decoupling, for the nanocomposites belonging to series 4 in Table 1 with n = 17 and 42. For comparison, the continuous line represents the DSC curve for the sample $[76]_{17}$[4]-II with arbitrary units along the y axis. Key: (□) $[76]_{17}$[4]-II-$\Delta\nu$; (○) $[76]_{17}$[4]-II-$\Delta\nu_{dec}$; (■) $[83]_{42}$[4]-II-$\Delta\nu$; (●) $[83]_{42}$[4]-II-$\Delta\nu_{dec}$; (△) $[76]_{17}$[4]-II-T_1^{-1}; (▲) $[83]_{42}$[4]-II-T_1^{-1}. The uncertainties in the ^{7}Li spin−lattice relaxation rates and line widths are approximately 5%.

−75 ppm characteristic of T^2 ($RSi^*(OSi)_2OH$) and T^3 ($RSi^*(OSi)_3$) sites (where R is the organic motif). They show the strong condensation of the silicon alkoxides and the formation of silica nodes which act as cross-linking units of the polymeric PEO network. Again, the presence of $LiClO_4$ does not disturb the hydrolysis−condensation process, and the NMR spectra are equivalent to spectra of salt-free samples.[9]

DSC and Ionic Conductivity. As for semicrystalline polymers and organic/inorganic systems, analyzing glass transitions for ormolytes is difficult. The DSC measurements for the samples $[58]_{12}$[4]-I and $[76]_{17}$[4]-II, shown in Figures 2 and 3, indicate that the PEG inside these two types of nanocomposites is in the amorphous state, since no melting transitions are observed in the thermograms. These DSC curves suggest also the presence of two second-order transitions for both samples. These two transitions could be associated with the biphasic character of the PEG inside the nanocomposites. The polymer far away from silica behaves as unrestricted PEG chains, possessing glass transition temperatures, T_g^{DSC}, at around −50 and −25

Table 2. Room Temperature Ionic Conductivity[a] for Different Sample Series

series 1:[b] $[X]_{20}$[4]-I	$[41]_{20}$[4]-I	$[58]_{20}$[4]-I	$[78]_{20}$[4]-I
σ (S/cm)	4.0×10^{-7}	8.0×10^{-7}	3.3×10^{-6}
series 2: $[58]_n$[4]-I	$[58]_6$[4]-I	$[58]_{12}$[4]-I	$[58]_{20}$[4]-I
σ (S/cm)	9.2×10^{-5}	3.5×10^{-6}	8.0×10^{-7}
series 4: $[X]_n$[4]-II	$[26]_2$[4]-II	$[76]_{17}$[4]-II	$[83]_{42}$[4]-II
σ (S/cm)	1.3×10^{-7}	1.5×10^{-6}	1.2×10^{-5}

[a] The uncertainties in the ionic conductivities are ca. 10%. [b] These samples are not shown in Table 1, however are similar to those of series 1.

°C, respectively for the nonbonded (type I) and bonded (type II) hybrids. On the contrary, the polymer near the silica nodes is more rigid due to physical interaction, type I, or covalent bond, type II, with silica, both showing transitions around 50 °C.

The respective plots of ^{7}Li line width as a function of the temperature are also shown in Figures 2 and 3. These plots are placed together in order to show that the transitions observed by DSC occur near the ^{7}Li NMR line width transitions. This topic will be discussed later.

Thermal properties of PEG/silica nanocomposites were previously studied.[14] Generally the T_g^{DSC} of type I ormolytes increases with the increase of the polymer chain length. Depending on the synthesis conditions (catalyst), increasing the weight percent of the polymer decreases or does not affect T_g^{DSC}. Unlike type I, type II materials show some decreasing T_g^{DSC} when the polymer chain length increases. Similar to silica-free polymer electrolytes,[15] types I and II nanocomposites exhibit an increase in the glass transition temperature with the increase of the lithium concentration. However, this behavior is less accentuated for nonbonded materials. For similar compositions, T_g^{DSC} values are always higher for type II materials, which is a consequence of the polymer motional hindrance introduced by the covalent bonds connecting the organic and inorganic phases.

These T_g^{DSC} trends are also corroborated by the ionic conductivity measurements[16,17] summarized in Table 2, where the values of σ are reported for various weight percents of polymer, X, and chain lengths, n, for both types I and II materials.

For both types of ormolytes, increasing X leads to some increase in the ionic conductivity. Increasing the polymer chain length, n, decreases the ionic conductivity for the nonbonded ormolytes, while an increase is measured for the bonded nanocomposites. Figure 4 presents the variation of the room temperature conductivity as a function of the ratio [O]/[Li] for both type I (series 3) and type II (series 5) samples. These two curves present similar shapes with a maximum for the ionic conductivity which is for [O]/[Li] values of 8 and 15 for series 3 and 5, respectively. This conductivity behavior as a function of the [O]/[Li] was previously reported and explained for nanocomposite systems[16,17] and pure polymeric ionic conductors.[36,37]

It was also observed,[16,17] only for the nonbonded ormolytes, a clear modification in the slope of the curve of conductivity vs temperature, around 50 °C, which could be related to the second thermal transition observed by DSC.

^{7}Li, ^{13}C, and ^{1}H NMR. Below the glass transition the ^{7}Li spectra consist of a very intense central transition ($-1/2 \leftrightarrow +1/2$) and an almost unobservably weak and

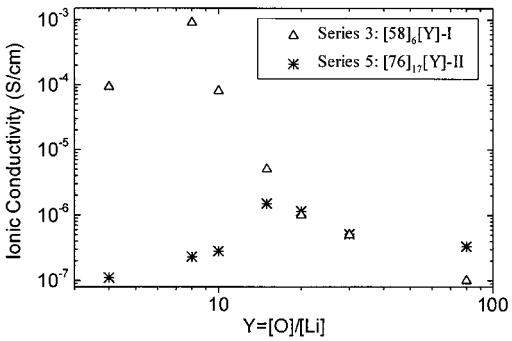

Figure 4. Behavior of the room-temperature ionic conductivity as a function of Y = [O]/[Li] for nonbonded (series 3, Table 1) and bonded (series 5, Table 1) samples. The uncertainties in the ionic conductivities are around 10%.

broad (∼5−10 kHz) line that could be associated with the quadrupolar satellite transitions ($^3/_2 \leftrightarrow {}^1/_2$ and $-{}^1/_2 \leftrightarrow -{}^3/_2$). Above the glass transition, the weak and broad line associated with the quadrupolar satellite peaks is averaged out as the temperature is raised from T_g. For this reason, only the ^{7}Li central transition was analyzed in this study. Despite well-resolved first-order quadrupole satellite lines having been already observed in solid polymer electrolytes utilizing the same experimental procedure used in this study (quadrupolar coupling $\nu_Q \sim 1$ kHz)[38] or using the quadrupolar-echo pulse sequence ($\nu_Q \sim 30$ kHz),[22] the quadrupole satellites lines are only faintly observed for the ormolytes. Since the experimental conditions applied at all temperatures assured a spectral bandwidth of at least 50 kHz, the absence of the satellite quadrupole powder pattern should be discussed. The absence of this structure, even in the rigid lattice limit, could be due to one of the following reasons: (a) distribution of electric field gradients with low quadrupole couplings ($\nu_Q \sim 1-10$ kHz), (b) highly symmetric lithium sites, or (c) very large quadrupole couplings ($\nu_Q \geq 100$ kHz). The two last hypotheses are not expected since highly symmetric sites or high quadrupolar couplings ν_Q are not observed for similar systems. In this case, the first reason could be true. Since the ormolytes are heterogeneous systems, it is expected that they present a wide distribution of electric field gradients, which results in a Gaussian-broadened satellite line. In addition, the satellite lines are broadened by the intense ^{1}H−^{7}Li dipolar interaction. Below the glass transition, where all transitions are broad, some of the central transition line broadening could also be due to first-order quadrupolar interactions incompletely averaged by rather slow motion. The central transition line broadening due to the second-order quadrupole interactions is expected to be very small since its estimated contribution,[20] ν_Q^2/ν_L, is on the order of hertz.

The ^{7}Li line width, with and without ^{1}H decoupling, and the spin−lattice relaxation time of the central transition were investigated as a function of temperature from −100 to +90 °C for all samples listed in Table 1. Typical results of these measurements can be seen in Figures 2 and 3 for types I and II nanocomposites with extreme values of the compositional parameter n, series 2 and 4, respectively. The curves for the different materials of each series present similar shapes but the characteristic parameters (T_g^{NMR}, T_{max}, line widths, ...) vary.

Taking as an example Figure 2, the line width evolution with temperature can be described by a curve

Table 3. Observed Trends for T_g^{NMR}, T_{max}, $\Delta\nu$, and $\Delta\nu_{dec}$ with the Increase of the *X*, *n*, and *Y* Parameters

	X series 1	*n* series 2	*Y* series 3	*n* series 4	*Y* series 5
T_g^{NMR} (°C)	approximately constant[a] $X < 80$: -32 ± 5 $X > 80$: -48 ± 5	increase $-37 \rightarrow -28$	approximately constant -38 ± 5	decrease $Y = 4$: $37 \rightarrow -11$ $Y = 15$: $-11 \rightarrow -17$	decrease $7 \rightarrow -16$
T_{max} (°C)	approximately constant $X < 80$: 30 ± 5 $X > 80$: 21 ± 3	increase $26 \rightarrow 46$	approximately constant 19 ± 5	decrease $Y = 4$: $81 \rightarrow 64$ $Y = 15$: $57 \rightarrow 46$	decrease $81 \rightarrow 43$
$\Delta\nu$ (kHz)	increase $5.4 \rightarrow 8.0$	approximately constant 6.4 ± 0.3	decrease $6.4 \rightarrow 2.7$	approximately constant $Y = 4$: 5.7 ± 0.2 $Y = 15$: 6.6 ± 0.1	increase $5.7 \rightarrow 6.7$
$\Delta\nu_{dec}$ (kHz)	increase $0.33 \rightarrow 0.76$	approximately constant 0.7 ± 0.1	decrease $0.59 \rightarrow 0.24$	approximately constant $Y = 4$: 0.8 ± 0.1 $Y = 15$: 0.30 ± 0.01	decrease $0.72 \rightarrow 0.29$

[a] For all the approximately constant parameters we show their (mean values ± standard deviations).

composed of two plateaus separated by a temperature range where rapid changes in line width occurs. The line width transition temperature is taken as the inflection point of these sigmoidal curves and the mean value of the temperatures, measured with and without proton decoupling, is named T_g^{NMR}. The uncertainty in T_g^{NMR} is ca. 15%. This characteristic glass transition temperature is around −30 °C and varies slightly with composition. Below T_g^{NMR}, the polymer is rigid and the rigid-lattice line widths will be denoted $\Delta\nu$ or $\Delta\nu_{dec}$, respectively, when measured without or with proton decoupling.

An additional broadening of the ^{7}Li line can also occur due to the finite life of the spins in any eigenstate as a result of the spin−lattice relaxation,[19] and this effect should be evident around T_{max}. In this situation, the spin−lattice relaxation rates can reach values on the order of ^{7}Li line width introducing a nonsecular line broadening. To estimate the lifetime broadening contribution to the ^{7}Li line width, the temperature dependence of the ^{7}Li spin−lattice relaxation rate of the central transition, T_1^{-1}, is also shown in Figure 2. These bell-shaped curves present maxima at T_{max} around 35 °C and indicate a small nonsecular broadening contribution to the ^{7}Li line width. Normally, this small nonsecular line broadening occurs at the same temperature range of the second thermal transition observed in the DSC curves, Figure 2, which could be associated with some transition of the more rigid PEG, such as a glass transition, resulting in a small line narrowing. For some nonbonded samples it is possible to observe both the line broadening, due to the T_1^{-1} maximization, and the small line narrowing, due to the second thermal transition, occurring at different temperature ranges. Similar effects can also be observed in the line width behavior of ^{1}H and ^{13}C nuclei of the sample $[73]_6$[4]-I shown in Figure 5. In the case of type II nanocomposites, this additional transition in the ^{7}Li line width around 50 °C is not observed, Figure 3. Modifications in the ^{13}C and ^{1}H line widths can be observed for sample $[76]_{17}$[4]-II only at approximately 75 °C, Figure 6.

The dependence of T_g^{NMR}, T_{max}, $\Delta\nu$, and $\Delta\nu_{dec}$ with the composition parameters *X*, *Y*, and *n* are generally weak and monotonic with respect to the composition parameters. The trends are summarized in Table 3 and will be discussed in the forthcoming section.

The activation energies for both relaxation processes were calculated.[22,31−33] In the case of line width, the activation energies were obtained from the measurements without proton decoupling, since there are few points to calculate these parameters from proton decoupled ^{7}Li line width. In the case of the spin−lattice relaxation, two values of activation energy were found in the temperature intervals above and below T_{max}. The values obtained for E_a are presented in Tables 4 and 5 for all samples of each series of ormolytes. The uncertainty in this parameter is around 15%. The samples $[58]_6$[4]-I, $[76]_{17}$[4]-II and $[76]_{17}$[15]-II were prepared several times, and the variation of the different values was calculated to be 15%.

To estimate the contribution of the polymer chain (PEG) to the ionic dynamics, ^{1}H and ^{13}C NMR experiments were performed, including line width and spin−lattice relaxation rate measurements as a function of temperature. Ormolytes of both types I and II, with similar compositions, $[73]_6$[4]-I and $[76]_{17}$[4]-II, were studied. These data are presented in Figures 5 and 6

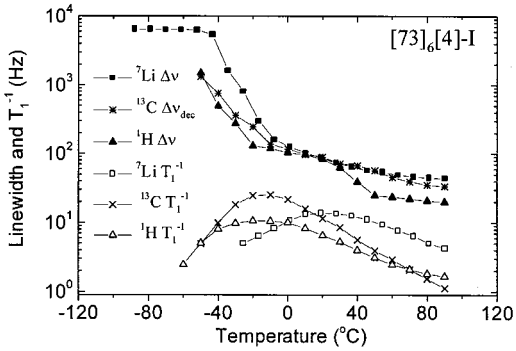

Figure 5. Temperature dependence of the ^{1}H, ^{7}Li, and ^{13}C line widths and spin−lattice relaxation rates for the sample $[73]_6$[4]-I. The uncertainties in the line widths and spin−lattice relaxation rates for ^{1}H, ^{7}Li, and ^{13}C are around 5, 5, and 15%, respectively.

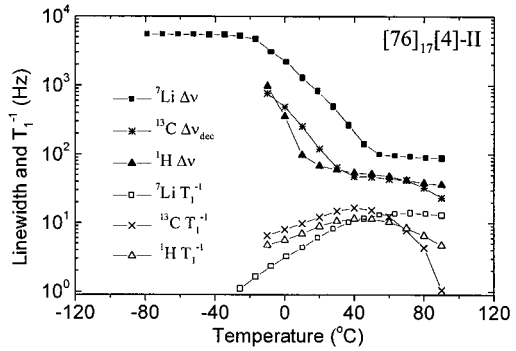

Figure 6. Temperature dependence of the ^{1}H, ^{7}Li, and ^{13}C line widths and spin−lattice relaxation rates for the sample $[76]_{17}$[4]-II. The uncertainties in the line widths and spin−lattice relaxation rates for ^{1}H, ^{7}Li, and ^{13}C are around 5, 5, and 15%, respectively.

Table 4. Activation Energies[a] Obtained from $\Delta\nu(T)$ and $T_1(T)$ Measurements for Materials of Type I

sample	from $\Delta\nu(T)$ E_a (eV)	from $T_1(T)$ E_a (eV) $T > T_{max}$	from $T_1(T)$ E_a (eV) $T < T_{max}$
	Series 1		
$[41]_6$[4]-I	0.52	0.18	0.13
$[58]_6$[4]-I	0.35	0.10	0.18
$[73]_6$[4]-I	0.65	0.23	0.18
$[78]_6$[4]-I	0.50	0.13	0.25
	Series 2		
$[58]_6$[4]-I	0.41	0.26	0.26
$[58]_{12}$[4]-I	0.41	0.25	0.28
$[58]_{20}$[4]-I	0.39	0.18	0.22
	Series 3		
$[58]_6$[4]-I	0.36	0.19	0.22
$[58]_6$[8]-I	0.34	0.22	0.25
$[58]_6$[10]-I	0.58	0.22	0.29
$[58]_6$[15]-I	0.44	0.19	0.23
$[58]_6$[30]-I	0.80	0.23	0.31
$[58]_6$[80]-I	0.37	0.20	0.31

[a] The uncertainties in the activation energies are approximately 15%.

Table 5. Activation Energies[a] Obtained from $\Delta\nu(T)$ and $T_1(T)$ Measurements for Materials of Type II

samples	from $\Delta\nu(T)$ E_a (eV)	from $T_1(T)$ E_a (eV) $T > T_{max}$	from $T_1(T)$ E_a (eV) $T < T_{max}$
	Series 4		
$[26]_2$[4]-II	0.64		0.26
$[76]_{17}$[4]-II	0.45		0.23
$[83]_{42}$[4]-II	0.51		0.24
$[76]_{17}$[15]-II	0.38	0.05	0.22
$[83]_{42}$[15]-II	0.59	0.08	0.20
	Series 5		
$[76]_{17}$[4]-II	0.45		0.23
$[76]_{17}$[8]-II	0.39	0.07	0.28
$[76]_{17}$[10]-II	0.49	0.04	0.21
$[76]_{17}$[15]-II	0.38	0.05	0.22
$[76]_{17}$[30]-II	0.40	0.10	0.36

[a] The uncertainties in the activation energies are approximately 15%.

together with those previously shown for the ^{7}Li nucleus to facilitate the comparison among the nuclei associated with the polymeric chain and that associated with Li^+.

For each material the line width and spin−lattice relaxation curves for ^{1}H and ^{13}C nuclei present similar behaviors and indicate that the polymer dynamics helps the ionic mobility. As for the ^{7}Li, the T_1^{-1} curves for ^{1}H and ^{13}C present bell-shaped curves, and the maxima of these two curves occur at the same temperatures, which are around 40 °C lower than the T_{max} of the Li^+ species. The ^{1}H line width evolution of type I material presents a three plateau evolution with the first transition near −40 °C and the second one above 30 °C, Figure 5. This is also observed for ^{13}C line width behavior, Figure 5. This behavior could be correlated with the thermal analysis that indicated the presence of two second-order transitions for these compounds. For type II materials it was possible to observe, for ^{1}H and ^{13}C nuclei, one intense transition around 0 °C and another very small around 70 °C, Figure 6. For both types of nanocomposites, the more intense transitions for ^{13}C and ^{1}H line widths occurred at temperatures between 20 and 30 °C lower than that found for the ^{7}Li cations. The comparison between the behaviors of the polymer backbone and the dissolved cations will be discussed in the next sections.

Polymer−Cation Interactions. The ^{7}Li line width was measured as a function of temperature for all the samples listed in Table 1. The results show that, independent of the decoupling condition, the line width transitions occur near the glass transition of the nanocomposites, Figures 2 and 3. Moreover, the ^{1}H and ^{13}C NMR measurements performed on two samples, $[73]_6$[4]-I and $[76]_{17}$[4]-II, show line width transitions starting at temperatures lower than those measured on the cation Li^+, Figures 5 and 6. These lower temperatures corresponding to the polymeric network dynamics are closer to the T_g measured by DSC measurements. Therefore, rapid cation motions occur only when the polymer segments motions are high enough to assist the cationic jumps.[1,2,16,39−41] This conclusion is corroborated by the measurements of ^{13}C and ^{1}H T_1^{-1} vs temperature, Figures 5 and 6. The results indicate similar behavior for type I and type II ormolytes. ^{1}H and ^{13}C nuclei belonging to the polymeric chain present T_1^{-1} maxima at similar temperatures while the ions Li^+ present a minimum of T_1 for temperatures which are approximately 40 °C higher.

The observation of stronger ^{7}Li and ^{1}H line narrowings above 30 °C for the nonbonded samples, Figures 2, 3, 5, and 6, is in accordance to the DSC, Figures 2 and 3, and temperature-dependent ionic conductivity[16,17] measurements. This correlation could indicate that the polymer mobility, for nonbonded samples, significantly increases after the second thermal transition improving the ionic conductivity above 50 °C, which does not occur for the bonded samples.

Below T_g^{NMR} the rigid-lattice ^{7}Li line widths, obtained with and without ^{1}H decoupling, demonstrate that the ^{7}Li−^{1}H magnetic dipolar interaction accounts for approximately 90% of all ^{7}Li spin interactions. Above T_g^{NMR}, a slight modification of the ^{7}Li line width with temperature is observed in several samples, Figures 2 and 3. This is a consequence of both the high spin−lattice relaxation rate, which reaches values on the order of the line width for higher temperatures (14 ± 1 Hz), and the second transition observed by DSC.

On the basis of the above discussion the polymer motion and the Li^+ ion diffusion cause the observed temperature dependence of both the ^{7}Li line width and spin−lattice relaxation time. Also, the ^{1}H−^{7}Li is predominately responsible for the temperature behavior of the ^{7}Li line width. However, other studies[22] indicate that the quadrupolar interaction is responsible for the ^{7}Li spin−lattice relaxation. The minimum ^{7}Li T_1 obtained for all samples are very similar showing an average value of 71 ± 7 ms. This fact indicates that the quadrupolar couplings and the ^{7}Li sites are also very similar for all of the samples.

The activation energies obtained from the curves of ^{7}Li line width for all ormolytes (Tables 4 and 5) present similar values to those found for silica-free ionic conducting polymers.[22] The activation energies obtained from the curves of ^{7}Li spin−lattice relaxation for nonbonded ormolytes (type I) show a three-dimensional BPP behavior, where the activation energies obtained above and below T_{max} are similar (Table 4). These activation energies present comparable values to those found for silica-free ionic conducting polymers.[22] However, in the case of the bonded ormolytes (type II), because of the hindrance to chain mobility by the

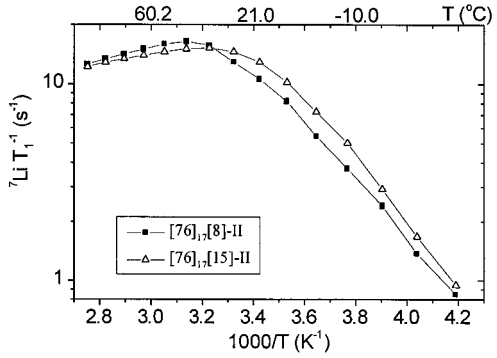

Figure 7. Arrhenius plot of the ^{7}Li T_1^{-1} for the bonded nanocomposites $[76]_{17}$[8]-II and $[76]_{17}$[15]-II. The difference between the slopes in the temperature intervals above and below T_{max} can be easily observed.

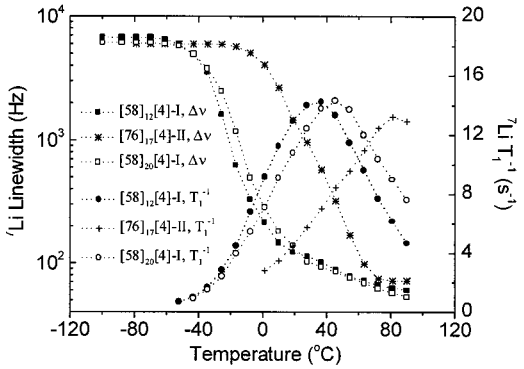

Figure 8. Temperature dependence of the ^{7}Li spin−lattice relaxation rate and line width without ^{1}H decoupling, for the nanocomposites $[58]_{12}$[4]-I, $[58]_{20}$[4]-I, and $[76]_{17}$[4]-II.

silica nodes, the difference between the activation energies obtained above and below T_{max} indicates a large deviation from the three-dimensional BPP model (Table 5). Figure 7 contains the most evident results showing this behavior for the bonded samples $[76]_{17}$[8]-II and $[76]_{17}$[15]-II. Because of the heterogeneity of mobility in different sites of the bonded polymer chain, another relaxation models should be used to understand this behavior, such as a distribution of correlation times (e.g., the Kohlrausch−Williams−Watts function)[42,43] and/or a quasi two-dimensional BPP.[44]

It is important to notice that the activation energies obtained from $\Delta\nu(T)$ are sensibly larger than those obtained from $T_1(T)$ measurements. These results indicate that a single relaxation model BPP cannot be used along the whole temperature interval. This result is reasonable because the activation energy necessary for the glass transition process is expected to be larger than that of the hopping process of the cation Li^+ above T_g.[22]

The general features discussed above for samples belonging to series 2 and 4 are also observed for the other type I and type II materials. This indicates that the ionic mobility occurs through similar mechanisms described for pure polymer electrolytes.[1] However, compositional variations (X, n, and Y) and dependence of the type of the material (I and II) are observed for the different NMR parameters (T_g^{NMR}, T_{max}, $\Delta\nu$, and $\Delta\nu_{dec}$) and will be discussed in the next sections.

Influence of the Compositional Parameters. The major trends of the ^{7}Li NMR spectral changes as a function of the compositional parameters are summarized in Table 3. The following general evidences are observed in this table.

(a) Type I Materials. (1) Effects of the Weight Percent of Polymer (*X*). Both T_g^{NMR} and T_{max} for nonbonded ormolytes are approximately constant with changes of the weight percent of polymer X (series 1). This effect suggests that the silica cluster surface is large and reduces the mobility of the organic phase through weak bonds between the polymer and the inorganic structure. For $X > 80$, the T_g^{NMR} and T_{max} present a decrease possibly due to the larger presence of an unhindered polymeric phase.

(2) Effects of the Polymer Chain Length (*n*). The increase of polymer chain length (series 2) is related to an increase of T_g^{NMR} and T_{max}. Such an increase in the rigidity is probably related to the increasing hindrance of chain motions with chain length, as it was already observed on the pure polymer.[14]

(3) Effects of the Lithium Concentration (*Y*). High lithium content in these materials (series 3) does not affect significantly T_g^{NMR} and T_{max}, which is rather different from silica-free polymer electrolytes, where T_g is dependent on the salt content.[22] Consequently, one can conclude that polymer−silica interactions overcome the effect of the Li^+ ions on the chain mobility.

(b) Type II Materials. (4) Effects of the Polymer Chain Length (*n*). The increase of the polymer chain length, n, (series 4) decreases both T_g^{NMR} and T_{max} for both lithium concentrations ($Y = 4$ and 15). This fact had been observed in type II nanocomposites without lithium by EPR and NMR experiments.[10] Polymer chains are bonded to the silica network by covalent bonds and the motion of the first segments is severely restrained. Therefore, for shorter PEG chains, the entire chain is near the silica node and the segmental motions are severely hindered. For longer PEG chains, only a small fraction of the chains is located near the silica interface and the majority of chains segments have high mobility.[10]

(5) Effects of the Lithium Concentration (*Y*). The effect of increasing the Li concentration (series 5) results in an expected increase for both characteristic temperatures T_g^{NMR} and T_{max}. Li^+ ions are complexed by the specific sites of the polymer chains (ether groups) and then act as reticulation nodes, with the consequence of reducing the segmental mobility of the PEG.

Bonded, Nonbonded, and Silica-Free Samples Correlation. Figure 8 presents the temperature dependence of the ^{7}Li line width without ^{1}H decoupling and ^{7}Li spin−lattice relaxation rate for three different nanocomposites $[58]_{12}$[4]-I, $[58]_{20}$[4]-I, and $[76]_{17}$[4]-II, which present similar parameters X, n, and Y.

The effect of the covalent bonding of the polymer chain to the inorganic silica structure (sample $[76]_{17}$[4]-II) is clearly apparent from $\Delta\nu(T)$ and $T_1^{-1}(T)$ data which show a large shift of the T_g^{NMR} and T_{max} toward higher temperatures relative to the type I ormolytes ($[58]_{12}$[4]-I and $[58]_{20}$[4]-I). This result is consistent with ionic conductivity measurements, Figure 4 and Table 2, which present systematically lower conductivity values for bonded ormolytes compared with the nonbonded materials of similar compositions. This confirms that the presence of covalent bonds between the silica structure and the PEG chains strongly hinder the polymer motion and consequently the Li^+ mobility, leading to an increase of T_g^{NMR} and a decrease of ionic conductivity. This interpretation is also confirmed by

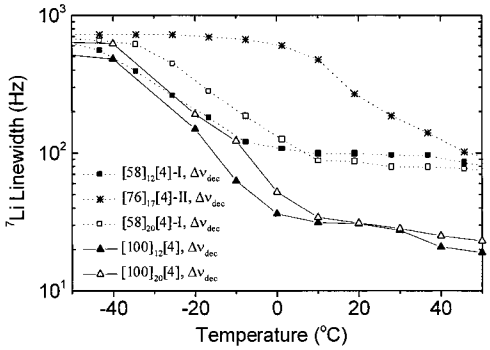

Figure 9. Temperature dependence of the ^{7}Li line width with ^{1}H decoupling, for the nanocomposites $[58]_{12}$[4]-I, $[58]_{20}$[4]-I, $[76]_{17}$[4]-II, $[100]_{12}$[4], and $[100]_{20}$[4].

DSC measurements which show that the T_g^{DSC} of the nonbonded sample, $[58]_{12}$[4]-I, is much lower than that of the bonded one, $[76]_{17}$[4]-II, revealing a much lower mobility of polymer chains in type II nanocomposites for similar temperatures.

Figure 9 shows the temperature dependence of the ^{7}Li line width with ^{1}H decoupling for three different nanocomposites, $[58]_{12}$[4]-I, $[58]_{20}$[4]-I, and $[76]_{17}$[4]-II, and, for comparison, also for two silica-free samples, $[100]_{12}$[4] and $[100]_{20}$[4], all presenting similar parameters *X*, *n*, and *Y*. Figure 9 reinforces the preceding conclusions: the presence of silica increases the glass transition of the PEG, this effect being more intense for the bonded ormolytes. Figure 9 also points out that the averaging of the line width due to the motional narrowing is less efficient for ormolytes when compared with silica-free samples. This effect indicates a restricted polymer motion resulting from the interaction of PEG with the silica structure through weak or strong bonds. Similar effects were also observed for PEO intercalated in clays.[45]

Conclusions

The dissolution of $LiClO_4$ inside nanocomposite structures provides materials with ionic conductivity that could reach values comparable with pure polymer electrolytes. Moreover, the mechanical properties of the nanocomposites are much better than the pure polymeric materials, which is a requisite feature for further applications.

NMR studies have been performed to probe specifically the behavior of the mobile ionic species and also the polymer chains for type I and II ormolytes. These combined experiments point out that strong correlations are observed between the behavior of the solid electrolyte and the mobile species. The ion mobility is still assisted by segmental motion of the polymer. The detailed study of the mobility processes point out some interesting differences between nonbonded and bonded ormolytes. In the type II family, a strong deviation from the BPP model is observed, which could be the consequence of the segmental mobility hindrance. On the contrary, nonbonded type I nanocomposites are quite similar to pure polymer, which indicates that organic−inorganic interactions are weak.

Acknowledgment. T.J.B. thanks F. Becker-Guedes and D.J. Harris for editing this manuscript. The Brazilian Agencies FAPESP, CNPq, and FINEP and Brazil−France project USP-COFECUB supported this research.

References and Notes

(1) Gray, F. M. *Solid Polymer Electrolytes, Fundamentals and Technological Applications*, 1st ed.; VCH Publishers: New York, 1991.
(2) Armand, M. *Adv. Mater.* **1990**, *2*, 278−286.
(3) Ratner, M. A.; Shriver, D. F. *Mater. Res. Soc. Bull.* **1989**, 39−51.
(4) Lightfoot, P.; Mehta, M. A.; Bruce, P. G. *J. Mater. Chem.* **1992**, *2*, 139−140.
(5) Boden, N.; Leng, S. A.; Ward, I. M. *Solid State Ionics* **1991**, *45*, 261−270.
(6) Judeinstein, P.; Sanchez, C. *J. Mater. Chem.* **1996**, *6*, 511−525.
(7) Novak, B. M. *Adv. Mater.* **1993**, *5*, 422−433.
(8) Ravaine, D.; Seminel, A.; Charbouillot, Y.; Vincens, M. *J. Non-Cryst. Solids* **1986**, *82*, 210−219.
(9) Judeinstein, P.; Titman, J.; Stamm, M.; Schmidt, H. *Chem. Mater.* **1994**, *6*, 127−134.
(10) Brik, M. E.; Titman, J. J.; Bayle, J. P.; Judeinstein, P. *J. Polym. Sci., Part B: Polym. Phys.* **1996**, *34*, 2533−2542.
(11) Schmidt, H.; Poppal, M.; Rousseau, F.; Poinsignon, C.; Armand, M.; Rousseau, J. Y. *2nd Int. Symp. Polym. Electrolytes* **1989**, 325−338.
(12) Brinker, J. C. *Sol−Gel Science, The Physics and Chemistry of Sol−Gel Processing*; Academic Press: San Diego, CA, 1989.
(13) Sanchez, C.; Ribot, F. *New J. Chem.* **1994**, *18*, 1007−1047.
(14) Judeinstein, P.; Brik, M. E.; Bayle, J. P.; Courtieu, J.; Rault, J. *Mater. Res. Soc. Symp. Proc.* **1994**, *346*, 937−942.
(15) Roux, C.; Gorecki, W.; Sanchez, J. Y.; Jeannin, M.; Belorizky, E. *J. Phys.: Condens. Matter.* **1996**, *8*, 7005−7017.
(16) Dahmouche, K.; Atik, M.; Mello, N. C.; Bonagamba, T. J.; Panepucci, H.; Aegerter, M. A.; Judeinstein, P. *Mater. Res. Soc. Symp. Proc.* **1996**, *435*, 363−368.
(17) Dahmouche, K.; Atik, M.; Mello, N. C.; Bonagamba, T. J.; Panepucci, H.; Aegerter, M. A.; Judeinstein, P. *J. Sol.-Gel Sci. Technol.* **1997**, *8*, 711−715.
(18) Lesot, P.; Chapuis, S.; Bayle, J. P.; Rault, J.; Lafontaine, E.; Campero, A.; Judeinstein, P. *J. Mater. Chem.* **1998**, *8*, 147−151.
(19) Slichter, C. P. *Principles of Magnetic Resonance*, 3rd ed.; Springer-Verlag: Heidelberg, Germany, 1990; Vol. 1.
(20) Abragam, A. *Principles of Nuclear Magnetism*; Oxford Science Publications: Oxford, England, 1996.
(21) Andrew, E. R.; Tunstall, D. P. *Proc. Phys. Soc.* **1961**, *78*, 1.
(22) Chung, S. H.; Jeffrey, K. R.; Stevens, J. R. *J. Chem. Phys.* **1991**, *94*, 1803−1811.
(23) Tunstall, D. P.; Tomlin, A. S.; MacCullum, J. R.; Vincent, C. A. *Phys. C* **1988**, *21*, 1039.
(24) Frank, H. P. *Polypropylene*, 1st ed.; Gordon and Breach Science Publishers: New York, 1968; Vol. 2.
(25) Rubin, I. D. *Poly(1-butene)−Its preparation and properties*, 1st ed.; Gordon and Breach Science Publishers: New York, 1968; Vol. 1.
(26) Komoroski, R. A. *High-resolution NMR spectroscopy of synthetic polymers in bulk*; VCH: Weinheim, Germany, 1986; Vol. 7.
(27) Bloembergen, N.; Purcell, E. M.; Pound, R. V. *Phys. Rev.* **1948**, *73*, 679−712.
(28) Gutowski, H. S.; Pake, G. E. *J. Chem. Phys.* **1950**, *18*, 162−170.
(29) Boyce, J. B.; Huberman, B. A. *Phys. Rep. (Rev. Sec. Phys. Lett.)* **1979**, *51*, 189−265.
(30) Hendrickson, J. R.; Bray, P. J. *J. Magn. Reson.* **1973**, *9*, 341−357.
(31) Berger, S.; Roos, J.; Brinkmann, D.; Chowdari, B. *Solid State Ionics* **1996**, *86−88*, 475−479.
(32) Cocciantelli, J.; Suh, K.; Sénégas, J.; Doumerc, J.; Pouchard, M. *J. Phys. Chem. Solids* **1992**, *53*, 857−859.
(33) Wang, G.; Roos, J.; Brinkmann, D.; Pasquali, M.; Pistoia, G. *J. Phys. Chem. Solids* **1993**, *54*, 851−855.
(34) Fyfe, C. A. *Solid State NMR for Chemists*, 1st ed.; CFC Press: Ontario, Canada, 1983.
(35) Gil, V. M. S.; Geraldes, C. F. G. C. *Ressonância Magnética Nuclear−Fundamentos, Métodos e Aplicações*, 1st ed.; Fundação Calouste Gulbenkian: Lisboa, 1987.
(36) MacCallum, J. R.; Vincent, C. A. In *Polymer Electrolytes Review*; MacCallum, J. R., Vincent, C. A., Eds.; Elsevier Applied Science Publishers: Essex, England, 1987; Vol. 1, pp 23−37.
(37) Julien, C.; Nazri, G. A. *Solid State Batteries: Materials Design and Optimization*, 1st ed.; Kluwer Academic: Boston, MA, 1994.

(38) Bonagamba, T. J.; Giotto, M. V.; Panepucci, H.; de Oliveira, A. L.; Sangiorge, C. L. *Bull. Magn. Reson.* **1996**, *17*, 94−95.
(39) Arumugam, S.; Shi, J.; Tunstall, D. P.; Vincent, C. A. *J. Phys.: Condens. Matter* **1993**, *5*, 153−160.
(40) McLin, M. G.; Angell, C. A. *J. Phys. Chem.* **1996**, *100*, 1181−1188.
(41) Müller-Plathe, F.; van Gunsteren, W. F. *J. Chem. Phys.* **1995**, *103*, 4745−4756.
(42) Williams, G. *J. Non-Cryst. Solids* **1991**, *131*−*133*, 1−12.
(43) Maring, D.; Meurer, B.; Weill, G. *J. Polym. Sci., Part B: Polym. Phys.* **1995**, *33*, 1235−1247.
(44) Küchler, W.; Heitjans, P.; Payer, A.; Schöllhorn, R. *Solid State Ionics* **1994**, *70*, 434−438.
(45) Wong, S.; Vaia, R. A.; Gianellis, E. P.; Zax, D. B. *Solid State Ionics* **1996**, *86/88*, 547−557.

MA991624W